On-chip fluorescence activated cell sorting by an integrated miniaturized ultrasonic transducer

Linda Johansson*, Fredrik Nikolajeff, Stefan Johansson and Sara Thorslund
Department of Engineering Sciences, Ångström Laboratory, Uppsala University, Box 534, 751 21 Uppsala, Sweden

ABSTRACT

An acoustic microfluidic system for miniaturized fluorescence activated cell sorting (µFACS) is presented. By excitation of a miniaturized piezoelectric transducer at 10 MHz in the microfluidic channel bottom, an acoustic standing wave is formed in the channel. The acoustic radiation force acting on a density interface causes fluidic movement and the particles or cells on either side of the fluid interface are displaced in a direction perpendicular to the standing wave direction. The small size of the transducer enables individual manipulation of cells passing the transducer surface. At constant transducer activation the system was shown to accomplish up to 700 µm sideways displacement of 10 µm beads in a 1 mm wide channel. This is much larger than if utilizing the acoustic radiation force acting directly on particles, where the limitation in maximum displacement is between a node and an anti-node which at 10 MHz is 35 µm. In the automatic sorting set-up, the system was demonstrated to successfully sort single cells of E-GFP expressing beta cells.

INTRODUCTION

The benefits of on-chip cell sorters as compared to macroscopic systems are several. Sample purity and the ability to handle infectious material in closed systems and integration with other steps are key motivations in addition to the ability to handle small sample volumes, the potentially lower cost and a lower requirement of trained operating personnel. The large-scale fluorescence-activated cell sorters, *FACS*, offer extreme cell throughputs (5 000 to 40 000 cells s^{-1})[1] and multi-parameter differentiation. However, cell sorters on-chip may not necessarily have to reach the same speed and the aforementioned benefits may be important enough to favor an on-chip alternative. If for example the total sample volume is small, it may not be of primary importance to complete the sorting in seconds as compared to a few minutes. In general, the throughput of microfabricated cell-sorters can be enhanced by building parallel systems which is possible due to their small sizes. If working with fragile mammalian cells, the ability to sort the cells into viable fractions is usually of much greater importance than having a high throughput.

To date, several techniques have been evaluated for on-chip continuous flow cell sorting. The most common of the *labeled* techniques for cell sorting, also referred to as single-cell sorting, are hydrodynamic sorting by switching valves,[2, 3] optical sorting,[4] electro-osmotic switching[5, 6] and electro-osmotic sorting in combination with pressure-driven flows.[7] Besides the labeled sorting, *label-less sorting* may be performed; also referred to as bulk sorting. By excluding the initial staining of the cells of interest, the number of process steps is advantageously reduced. Most often the bulk sorting tend to provide a sample enriched in target cells rather than a homogenous cell population.[8] The label-less separation is limited to a physical difference between the cells such as size[9, 10] or optically induced polarization,[11, 12] electrically induced polarization[13] or acoustic contrast factor relative the medium[14] (see the *Theoretical Model* section for an explanation of the acoustic contrast factor). Generally, few cells display strong physical differences and labeling based on immunological properties[15] is therefore necessary in many applications. Separating by the use of immunologically labeled magnetic beads is a commercially popular separation method and may be classified as bulk sorting with requirement of an initial labeling step. As opposed to fluorescent tagging, the magnetic bead may be undesired in a following step and needs to be removed, which may be detrimental to the cell. For this reason the beads are often used in negative selection.[8] The method evaluated in this article is of type labeled sorting.

Most methods for on-chip cell sorters presented in the literature display some draw-backs. The hydrodynamic systems are often very sensitive to small changes in hydrodynamic pressure, for instance resulting from deviant levels of fluid in reservoirs. For various electrokinetic sorting techniques, buffer incompatibilities can be an issue depending on the ion strength and pH required and additionally joule heating needs to be controlled.[2] Moreover, the conditions may change during the sorting process: e.g. electro-osmotic induced flows will be affected by changed electrical charge of the channel walls as a result of non-specific adsorption.[2] The strength of the electrical fields required may also be high enough to affect the viability of

sensitive cells.[2] While the conventional macro-scale FACS uses electrical fields during the cell sorting step, the cells are for the most commonly used set-up enclosed in charged droplets before being deflected in an electrical field. For extra high demands of cell recovery negative sorting is employed, i.e. only unwanted droplets are deflected while the desired droplets move straight ahead.[1] A sorting method that has achieved much attention recently is optical sorting, but the high light intensity levels employed are related to viability issues since not only temperature increase but also photodamage 'optocution'[16] are direct effects of the light. Optical sorting, weather the optical system is located off- or on-chip requires beam shaping objects[17, 18] and an extra optical beam branch besides the one for fluorescence detection. Furthermore, it is advantageous if the sorting method is insensitive to cell properties other than the one employed for sorting. For optical sorting the refractive index may vary within a cell and the optical force may therefore affect the cell dynamics[18] and generate a diverse response. Regarding dielectrophoretic polarization parameters such as the cell morphology, the cell differentiation and the cell physiological state contribute to a large degree and therefore generate a diverse result.[8] Insensitivity to cell parameters may be achieved if the force acts not on the particles themselves but on the fluid, as in hydrodynamic sorting or as in the acoustic sorting method presented here where the force acts on the fluid rather than on the particles. In conclusion, there is a demand for on-chip sorting methods that offer robustness, less stringent requirements on buffers, gentle sorting principle and simple integration.

Sorting speeds for on-chip cell sorting devices as calculated from the given switching times are in the range of hundreds of particles per second for reported hydrodynamic[2, 3] and optical sorting[4] systems. Directly measured sorting speeds in the range of tens of particles per second are reported for systems based on dielectrophoretic,[13] optical,[12] electro-osmotic[19] and hydrodynamic[2] forces. Lower values of directly measured sorting speeds, in the range of single cells per second, are reported for optoelectronic[20] and electro-osmotic[6] systems with emphasis on features such as gentleness and high-resolution detection, respectively.

Acoustic forces for separation in continuous flow has been employed in label-less mode, for separating different kinds of particles [14, 21] and for separating particles from a fluid[22-25] based on the size and the acoustic contrast factor relative the fluid. Batch-wise sorting has been shown by selectively trapping the cells of interest by means of an acoustic transducer and re-directing the flow and hence the trapped cells to a different channel output.[26, 27] A labeled set-up has been proposed where an acoustic transducer is intended to block the particles from entering one of two fluid outlets.[28] In several studies acoustic manipulation is recognized as a gentle manipulation method also for long-term handling such as in acoustic trapping.[29, 30] The viability of cells has been evaluated for this exact platform (only with smaller transducer),[31] for instance neural stem cells after 15 minutes trapping (7 Vpp, 12 MHz) against a flow of 1 µL/min (26 mm/s) with no indication of viability loss as measured by Acridine-Orange staining of the cells. The manipulation performed here is expected to be gentler than the long-term trapping and the hydrodynamic drag from displacing the particles is not expected to add stresses to any large extent.

The method and set-up presented here enables large sideways (x-direction) particle displacements and individual particle manipulation by a small transducer integrated in the channel bottom of a glass and epoxy-based device. An acoustic standing wave above the transducer generates radiation forces on an interface between two fluids of different density, resulting in a repeatable mixing pattern of the two initially laminar flows.[32] Particles on either of the fluid interface are consequently displaced due to the drag force of the fluid that moves due to the acoustic radiation forces. To the authors' knowledge, this method to displace and hence to sort particles has not been presented before. As opposed to systems exploring the acoustic radiation force on particles, the maximum displacement is here not limited to a quarter of a wavelength, i.e. the distance from a pressure node to a pressure anti-node. For a system operated at 10 MHz that distance would be approximately 35 µm and for a 3 MHz system 100 µm. Large displacement is desirable for sorting since it enable less strict requirements on the fluidics at the outlets. In addition, separating several kinds of particles in a sample is possible by deflecting particles into multiple outlets by applying different voltage levels to the transducer. Thirdly, the large displacements enable the use of a low voltage signal thereby minimizing the temperature increase in the channel. The direction of the particle displacement is parallel to the transducer surface (x-direction), hence allowing for easier observation and also that the transducer can be mounted in the bottom channel wall which is compatible with microsystem manufacturing techniques. Other ways to obtain separation is by displacing the particles in the out-of-plane direction[33] or by exciting a fluid channel mode by an external transducer.[22, 34] In order to manipulate cells individually in a flow, the acoustic energy needs to be localized to a small zone as is obtained for the integrated miniaturized transducers.

EXPERIMENTAL DETAILS

Device fabrication

A schematic view of the platform is shown in Figure 1A and 1B. Miniature single layer PZT (lead zirconium titanate) transducers, 900×900×200 µm, were integrated into the channel bottom. The microtransducers were diced out from a 200 µm thick commercial piezoelectric Pz-26 plate

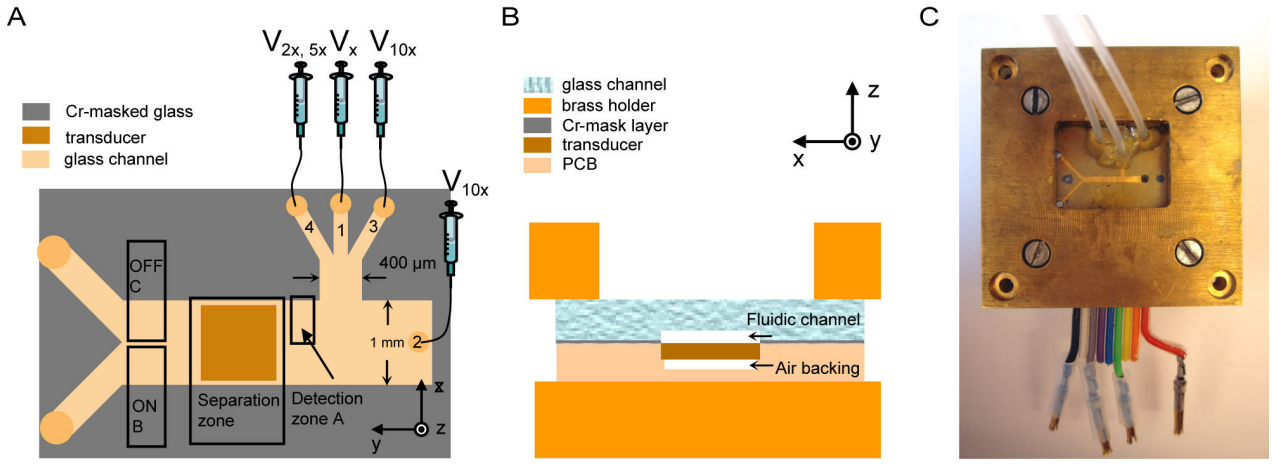

Figure 1. Top view of the platform showing the glass channel layer and the underlying PCB layer with integrated transducers (A) schematic and (C) photo. (B) shows the cross-section. The sample flow (1) and the shuffle flow (4) are indicated as well as the relative flow proportions. In the automatic separation a particle is detected in the *Detection zone A*. Particles are displaced upon transducer excitation in the *Separation zone* and exit in the *ON* zone B, while otherwise transported into the *OFF* zone C. The cavity was pressure sealed between two tightened brass plates.

(Ag-evaporated electrodes, Ferroperm, Kvistgard, Denmark). The transducers were mounted on a printed circuit board, PCB, (1.5 mm thick, 35 µm Cu coating) by conducting silver paint. Epoxy was cast around the transducers and the device was cured upside down on a polymer film at 90 °C for 24 hrs. The surface was carefully polished with 1200 grit silicon carbide paper, and through-holes for fluidic connections were drilled in the PCB plate. Finally the top electrode was deposited by evaporating 15 nm Cr followed by 150 nm Au. A 5 µm thick parylene C coating (Para Tech Coating Scandinavia AB, Sweden) was added in order to protect the metal surface during channel re-assembly and also to prevent contact between the sample and the epoxy. This coating step improved the biocompatibility of the device since both glass and parylene can be considered as inert materials, with parylene C even being classified as a Class VI polymer by the United States Pharmacopeia.[35]

The channel-reflector structure was fabricated by wet etching borosilicate glass wafers (Emmaboda Glasteknik, Sweden) to a reflector (channel roof) thickness of 994 µm and a channel depth of 71 µm. The etch solution consisted of HF:HNO_3:DI water (100:28:72, v/v) with 100 nm Cr and 2 µm 1813 resist (Shipley, Coventry, UK) as etch mask. The etch bath was ultrasonicated at repeated occasions in order to achieve even etching. Inlet holes in the glass reflector structure were drilled with a diamond drill. Before and after drilling, the etched glass structure was heated to 600 °C and slowly cooled down in order to reduce any induced stress. Fluidic connections on the PCB back side and glass front side were provided by connecting polyethylene tubings of 0.38 mm inner diameter (Intramedic BD, Sparks, MD) with epoxy. The glass-PCB device was sandwiched between two brass plates and pressure-sealed by screwing the upper and lower plates tightly together. A hydrogel was applied on the outer edges of the glass structure to facilitate the aligning procedure.

The channel was evaluated with four inlet flows and two outlet flows, see Figure 1A. The primary sample flow (1) with sheath flows (3) and (4) entered the cavity through the glass, see Figure 1C, while the positioning flow (2) and the outlet flow traversed the PCB plate to the backside. The sample flow was small and therefore all particles entered the main channel at approximately the same x-position. The flow (4) has a different density than the other 3 flows and is labelled ‘shuffle flow’ since its movement relative the sample fluid interface causes the particle displacement in x-direction. The many inlets give a high degree of flexibility in positioning the density interface and the particles (in x-direction) in relation to the acoustic field above the transducer which varies across the transducer surface (xy-direction).

Set-up and quantification

We used a solution of 17 % glycerol (Alfa Aesar, Karlsruhe, Germany) in DI water as shuffle fluid. The fluid contained 0.1 mM Rhodamine B (MP Biomedicals, Eschwege, Germany) to enable easy visualization of the fluidic behavior in the system. If not otherwise stated, the positioning fluid (2) and one of the sheath fluids (3) consisted of DI water, all connected to equal sized Hamilton syringes. A single syringe pump (Univentor Limited 864) was used to drive all syringes simultaneously. A total volume flow in the main channel of 6.9-104.0 µL min^{-1} (1.6-24.7 mm s^{-1}) was evaluated, corresponding to a Reynold’s number of 0.2-3. The

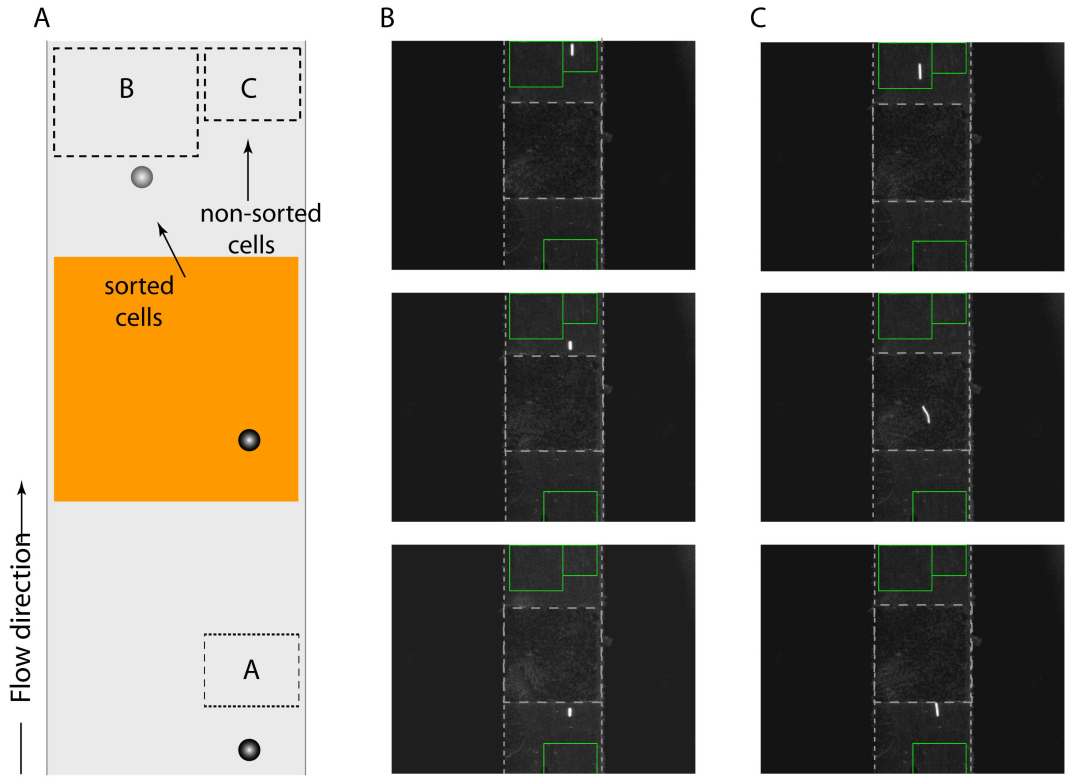

Figure 2. (A) Schematic view of the automated sorting principle of the system. The excitation of the transducer (orange rectangle) is controlled by the optical fluorescent detection of a cell in detection zone A. The time until excitation and the length of excitation was set to depend on the flow velocity in the system. For evaluation of the sorting yield, the cells were further identified in the two zones B and C. (B) Images from the software program controlling the automated system showing a non-sorted 10 µm bead and (C) a sorted bead (bottom to top).

fluorescence was induced by an Hg-lamp and was imaged using an inverted Nikon TE-2000-U microscope with a high sensitive cooled CCD camera (SPOT Diagnostic Instruments). In the acoustic zone the particles may be displaced into a different flow stream if the transducer is activated, and therefore exiting through a different outlet at the flow-split. Hence, sorting was performed by displacing particles or by letting them continue in the initial flow stream. The sideways (x-direction) displacement of particles was quantified as a function of the fluid flow velocity at a position 500 µm downstream from the excited transducer. Measurements were performed with 9.9 µm and 1.9 µm co-polymeric particles (Duke Scientific Corp.) dissolved in 17 % glycerol/DI water. The particles emit green fluorescence and can hence be studied separately from the red fluorescence emitting Rhodamine B labeled shuffle flow. To avoid particles adhering to each other, 0.5 % (v/v) Tween was added to the polymeric bead solution. A sample flow consisting of fat globules in water (1.5 % milk) was used to study the movement of particles with negative acoustic contrast factor, i.e. particles that are attracted to pressure anti-nodes. In addition to bead sorting, the system was evaluated for cell sorting with E-GFP transfected MIN6 β-cells. The E-GFP expressing β-cells were provided in DPBS-buffer at a concentration of about 1×10^6 cell mL^{-1}. During cell sorting, the device was run with DPBS as positioning fluid (2) and sheath fluid (3), Figure 1A, instead of DI water. Automatic switching was performed by the use of a custom built Labview software program (8.2.1, National Instruments). At 40x magnification, the image covered both an identification zone (A, Figure 2A) and two output zones (B and C, Figure 2A), thereby enabling on-chip sorting evaluation. The sample fluid is small which makes the particles enter the main channel at the same x-position. Upon detection of a fluorescently labeled incoming particle or cell in the zone A, a sinusoidal signal was applied to the transducer with a delay time corresponding to the time required for the cell to reach the transducer. A cell was identified when the intensity within the zone exceeded a threshold value. Approximately 10 images s^{-1} were processed by the program depending on the set exposing time. The automatic switching was evaluated by displacing every second particle and detecting the displaced particles in the zone B, Figure 1A, as well as the particles not subjected to displacement in the zone C. The length of the zones

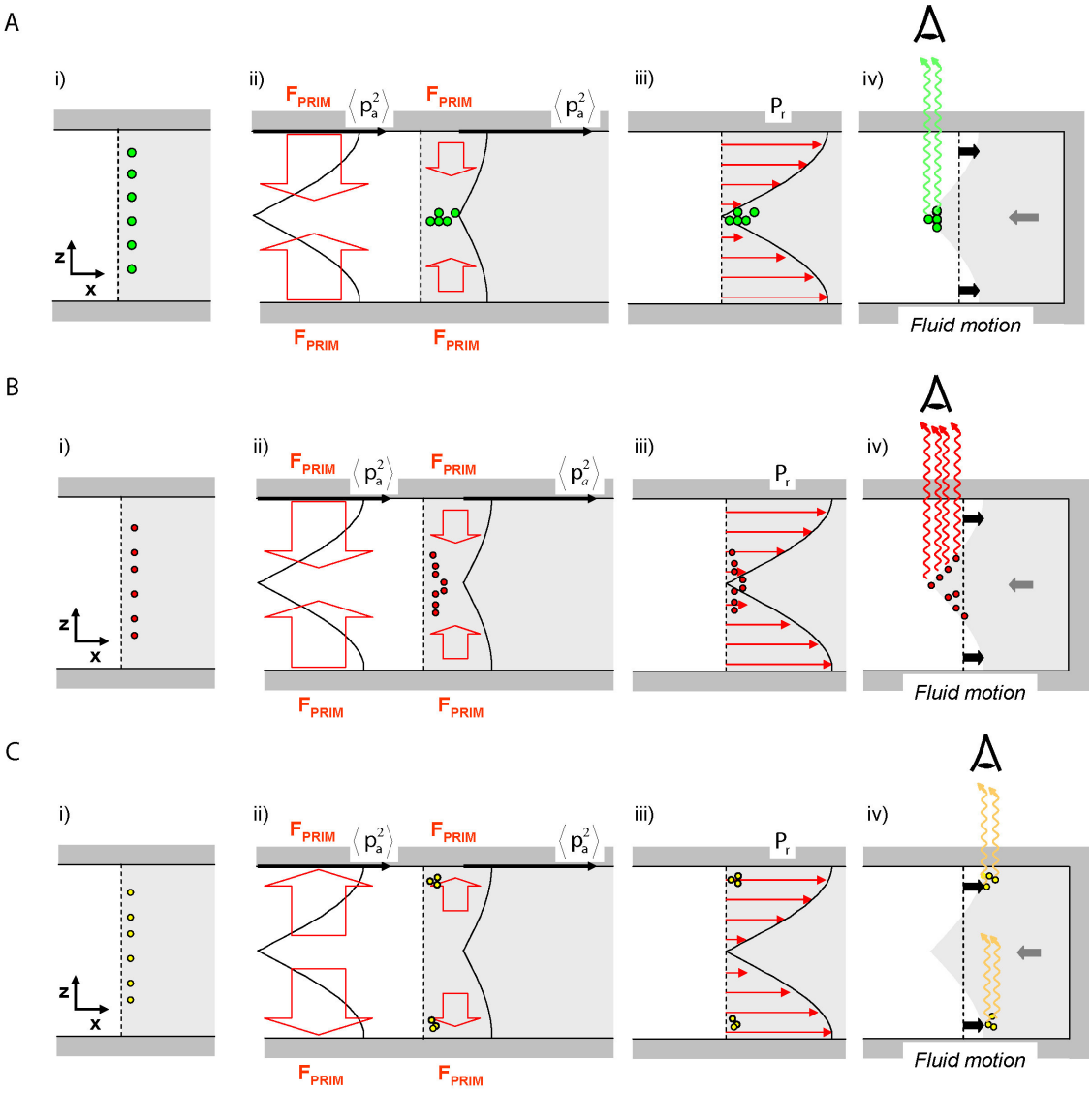

Figure 3. Illustration of the motion mechanisms for particles with (A) high acoustic primary radiation force, (B) lower acoustic radiation force as in the case of small particles or particles with low acoustic contrast factor and (C) particles with negative acoustic contrast factor attracted to the pressure anti-node as in the case of lipid cells. (i) The initial position of particles relative an interface between a lower-density fluid (white) and a higher-density fluid (grey), (ii) the time-averaged squared pressure amplitude in a standing wave and the primary radiation force that moves the particles to a pressure nodal plane in the middle of the channel, (iii) the radiation force acting on the interface and (iv) the expected initial displacement of the fluids and the displacement of particles due to the radiation force (black arrows) and due to conservation of mass flux (grey arrow).

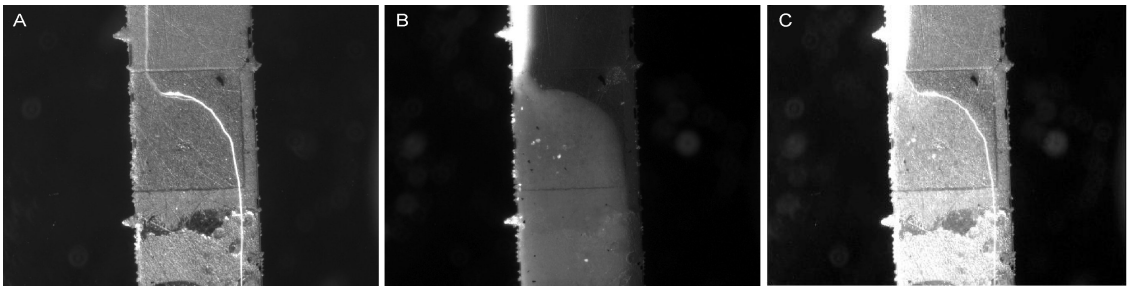

Figure 4. (A) Particle trajectories of fluorescent 10 µm particles at a total flow velocity of 1.6 mm s^{-1} during continuous transducer activation, (B) fluid distribution of the fluorescently labeled higher-density shuffle flow and (C) the two superimposed images for comparison.

optimized to be large enough to recognize a particle at the selected fluid flow and small enough not to count two cells as one. The optimizing of the lengths of the zones is complicated by the fact that particles travelling at different height in the channel have different speed (before pre-focusing). With the present channel dimensions, the velocity of 10 µm beads transported at the outermost top or bottom (z-direction) is only about 30 % of the velocity for beads traveling in the centre of the channel.[7] The solution was to close the window of recognition during 0.15 s after identification of a cell, thereby assuming cells in the sample to be adequately separated when entering the platform. Since the particle velocity is higher in the middle of the channel, the sorted identification zone B was set larger than the other two zones.

The transducer was excited by a high-frequency function generator (3320A from Agilent) and the driving voltage at the transducer was 8 V_{pp} unless stated otherwise. This excitation signal was decreased at low flow velocities in order to avoid the competitive effect of acoustic trapping of cells.

THEORETICAL MODEL

Upon activation of the ultrasonic field, the fluids are subjected to an acoustic radiation force at the fluid-fluid density interface that will cause convective motion of the fluids, as recently described by our group.[32] Particles present in any of the fluids adjacent to the density interface will move with the flow motion. A density difference in the range of a few percent (> 2 %) is required between the shuffle flow and the sample flow to generate effective fluid motion sufficient for cell sorting purposes. The primary acoustic radiation force acting on a fluid interface,[36]

$$F_{prim,I}(x) = iAQ_{SW}\frac{\left\langle \left| v_t^2 \right| \right\rangle}{2}\cos^2\left(\frac{2\pi}{\lambda/2}z\right)\left(\rho_{01} - \frac{Q_2}{Q_{SW}}\rho_{02}\right),$$

will cause a movement of the fluids perpendicular to the fluid interface (x-direction), in our case in the x-direction in Figure 3. λ is the wavelength of the acoustic wave, v_t is the oscillation velocity of the acoustic wave at the transducer surface, ρ_{01} and ρ_{02} are the densities of the fluid 1 and 2, respectively, in the absence of sound, i is the number of interfaces, A is the area of the interface and z is the direction of the wave propagation. Q_{SW} is the quality factor of resonance in the channel with fluid 1 and Q_2 is the quality factor with fluid 2. The above expression assumes a stepwise density difference at an interface and the force will be reduced as the density difference decreases due to the convective motions caused by the radiation force. The viscous forces have been omitted for simplicity. Equation (1) can be visualized by the schematic model illustrated in Figure 3 where a driving frequency matching a standing wave in the lower-density fluid is assumed. The higher-density shuffle flow is marked as the darker field. The top and bottom layers (z-direction) experience the highest radiation force due to higher time-averaged pressure amplitude, which is directed towards the fluid of higher density. Due to the conservation of mass flow, a flow in the opposite direction is expected to occur in the middle region where the acoustic radiation force is weaker.

A particle in the fluid will follow the flow since a deviation from the fluid velocity will generate a force according to Stoke's drag force, F_S,[37]

$$F_S(x) = 6\pi\eta r v_x^F,$$

here expressed for a particle velocity relative the fluid velocity, v_x^F, in the mixing direction x. η is the absolute viscosity of the fluid and r is the radius of the particle.

In addition, primary radiation forces on the particles will cause a pre-alignment in the axial z-direction. The primary radiation force on a particle may be expressed as follows,[38]

$$F_{prim,P}(z) = \frac{4\pi r^3}{3} f p_a^2 \left(\frac{\pi}{2\rho_0 c_0^3}\right)\left(f_1 + \frac{3}{2}f_2\right) sin\left(\frac{2\pi}{\lambda/2}z\right)$$

where r is the radius of the particle, p_a is the sound induced pressure amplitude, ρ_0 is the density of the medium in the absence of sound, c_0 is the speed of sound of the medium and f_1 and f_2 are defined as

$$f_1 = 1 - \frac{\rho_0 c_0^2}{\rho c^2} \text{ and } f_2 = \frac{2(\rho - \rho_0)}{2\rho + \rho_0}.$$

where ρ is the density of the particle and c is the speed of sound of the particle. The parenthesis containing the f_1 and f_2 is referred to as the acoustic contrast factor. Illustration of particles' motion in the acoustic zone above the transducer is shown in Figure 3. If the acoustic radiation force on the particles is strong, the particles align fast in the vertical direction as shown in Figure 3A. If the pre-focusing is not strong enough to enable positioning of the particles at a single vertical position at the initial stages of the fluid movements, Figure 3B, the particles will have different trajectories depending on a slight difference in entrance position. Hence, a divergence in the exit position is expected. A weaker pre-focusing is expected for smaller particles, for particles with low acoustic contrast factor and for higher fluid flows (i.e. shorter residence times above the transducer). Regarding particles with the opposite contrast factor, Figure 3C, for instance lipids, the acoustic radiation force will attract the particles to the pressure anti-

nodes and they will be displaced as the fluid at the channel top and bottom (z-direction), i.e. in the opposite direction relative the particles with positive acoustic contrast factor.

RESULTS AND DISCUSSION

Standing wave cavity

The standing wave cavity was evaluated by identifying the frequency of maximum displacement of the fluid interface, at which frequency the following measurements were performed. The optimal driving frequency was identified as 10.3 MHz. According to simulations of the fluid and reflector thicknesses[32] (given sound velocity$_{water}$ = 1500 m s^{-1}, sound velocity$_{reflector}$ = 5530 m s^{-1} and acoustic impedance$_{reflector}$ =14000 Ω) 10.3 MHz is a system resonance frequency. Still a prediction of an optimal driving frequency is complex due to the 3D characteristics of the acoustic field.

Particle displacement at the fluid interface

Figure 4A shows the displacement trajectory of 10 µm polymeric particles for a total fluid flow of 1.6 mm s^{-1} at continuous transducer activation. The exit position was displaced 730 µm relative the entrance position. The distribution of the high-density shuffle flow labeled with Rhodamine is shown in Figure 4B. By superimposing the two images in Figure 4C, it is evident that the particle trajectory correlates with the fluid motion. This behavior agrees with the model discussed in the previous section. It was also found that the particles can be dissolved in either the lower or the higher density fluid, i.e. the particles were displaced to a satisfactory degree independently on what side of the density interface they were positioned prior to the acoustic zone. As a result, the flexibility is large regarding cell medium. The level of pre-alignment (z-direction) is expected to be stronger in the resonance matched fluid (in our case the fluid of lower density), but no apparent differences in the effect were observed in the measurements.

In Figure 5, the water-based fluid, an emulsion of fat globules (homogenized milk), was fluorescently stained with fluorescent Rhodamine B and the higher-density shuffle-fluid was non-labeled. The fat globules have negative acoustic contrast factor and pre-align to the channel top and bottom (z-direction). Hence, they may be used as a marker for the fluidic movements at the top and bottom of the channel. Upon transducer activation, the sample fluid was observed to move towards the higher-density shuffle fluid (white arrow) but more evidently in the middle of the channel being pushed by the shuffle fluid into the middle of the channel (black arrow), Figure 5B.

Further, the fat globules were observed to be trapped and hence their position could be easily observed by a strong fluorescent signal. The trapping occurred at the top and bottom in the channel as expected. The trapping initiated at the edge of the channel in agreement with the top and bottom fluidic layers moving towards the high-density shuffle fluid, Figure 5C. The observations support the acoustic model presented above. After the initial stages of fluid motion, the trapping of fat globules was observed to occur also further towards the middle of the channel, see Figure 5D.

Flow dependence and pre-alignment dependence

The degree of particle displacement was evaluated for increasing fluid velocities, for a small shuffle flow, V_{2x}, and for a larger shuffle flow, V_{5x}, where x is the sample volume flow. The sorting speed was calculated by assuming a sample concentration with exactly one cell above the transducer at any time. The residence time, i.e. the time for a particle to pass the acoustic zone, was expected to influence the level of displacement. Accordingly, a lower level of displacement was observed for high, compared to low, flow velocities as shown in Figure 6. For example, at the total particle velocity of 27 particles s^{-1} the particle displacement was 220 µm and at 2 particles s^{-1} the displacement was 650 µm. The level of displacement was observed to depend on the entrance position. A larger displacement was observed for an initial position close to the channel wall as long as the shuffle fluid did not constitute a negligible portion of the fluid volume, in which case the density difference step was fast depleted and no strong effect was observed. Deviation from the trend curve at low flow velocities is expected due to the finite width of the channel. Generally, agreement with the trend curve requires that the mixing velocity is constant in time since otherwise the finite time spent in the acoustic zone will give different effect at different flows. Hence, a factor such as depletion of density difference after the same fluid segment being exposed to the ultrasound for long times also causes deviation.

An important parameter in cell sorting is the sorting yield. Above a certain total flow velocity (about 5 mm s^{-1}), the exit position of the particles start to vary, as seen in Figure 7. Despite having similar entrance positions in the x-direction, the particles have different trajectories across the transducer (xy-direction) and are hence not displaced to the same extent. In these cases the acoustic radiation force is not large enough to enable complete pre-alignment (z-direction), *Equation 3*, for very short residence times. At 8.8 mm s^{-1} flow conditions, the exit positions for 10 µm beads were distributed across approximately 120 µm, which was twice the entrance sample width. Since the acoustic radiation force and thus the pre-alignment is proportional to the particle volume, the divergence in exit positions also increased with smaller particles. For 2 µm beads and a flow velocity of 1.6 mm s^{-1}, the variation in exit position was found to be 150 µm as compared to no

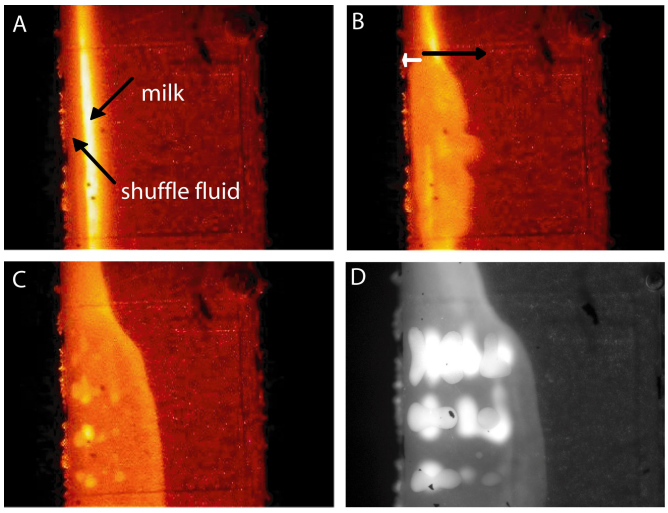

Figure 5. (A) Fluorescently labeled milk positioned to the right of the non-fluorescent shuffle flow (the flow entering from above). (B) In analogy with theory it was observed that, at the channel top and bottom, the milk upon transducer activation moved towards the higher-density shuffle fluid (white arrow). In the middle of the channel it was observed to move in the opposite direction since it is pushed by the shuffle fluid (black arrow). (C) The fat globules in the milk (bright) have negative acoustic contrast factor and pre-align to the top and bottom (z-direction). Hence, they may be used to visualize the fluidic motion at the top and bottom of the channel. The acoustic trapping of fat at the channel top and bottom was observed to initiate far into the higher-density shuffle fluid (bright spots). (D) The same phenomena imaged at higher magnification with focus at the channel top. The total flow velocity was 1.6 mm s^{-1}.

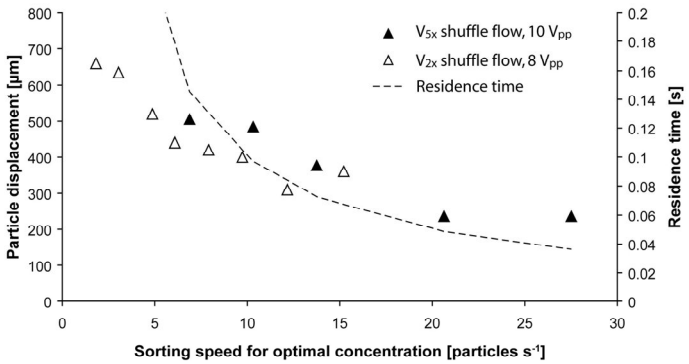

Figure 6. Displacement for 10 µm particles versus the sorting speed obtained by assuming a sample concentration with exactly one cell above the transducer at any time, for the fluid flow range of 1.6-24.7 mm s^{-1}. The particle displacement was evaluated at 10 V_{pp} and a shuffle flow V_{5x} (▲) and for 8 V_{pp} and a shuffle flow if V_{2x} (Δ), respectively (x being the sample volume flow). The calculated time for a fluid volume above the transducer, i.e. the residence time, is included (dotted line).

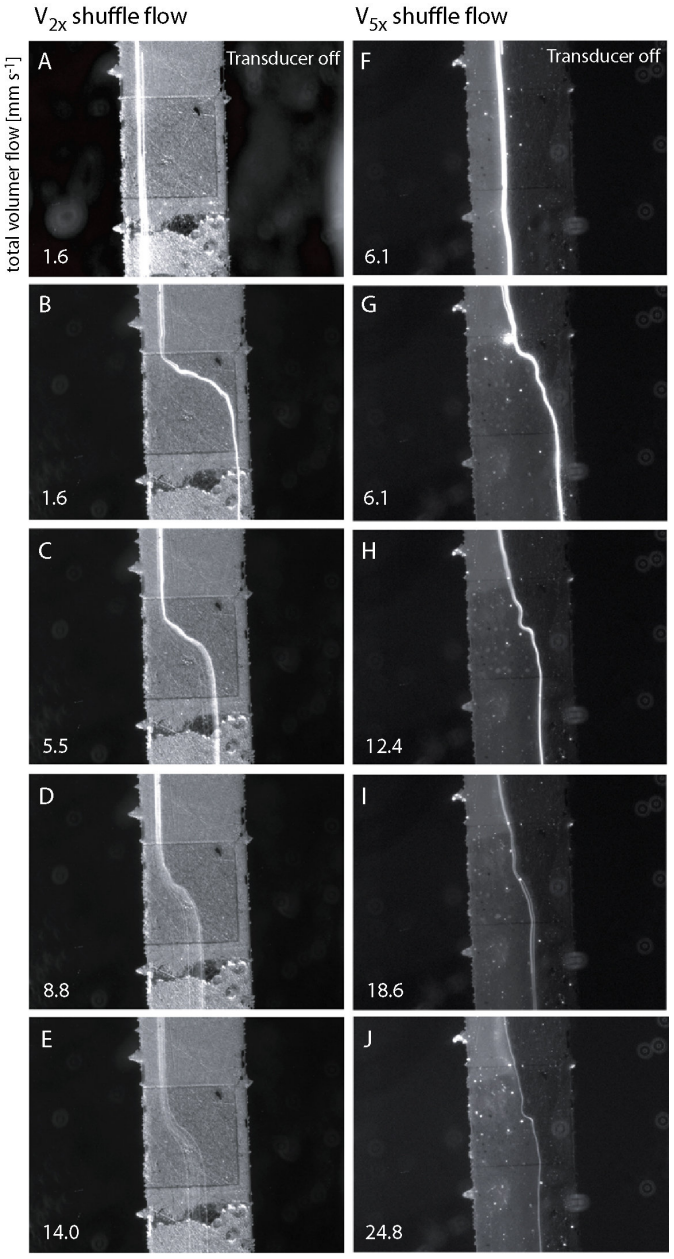

Figure 7. Images at 40x magnification of the particle trajectories for increasing flow velocities for (A-E) 8 V_{pp} and V_{2x} shuffle flows and for (F-J) 10 V_{pp} and V_{5x} shuffle flows (V_x corresponds to the sample volume flow). The total flow velocity in the system is given in every image (flow from the top). The fluorescence signal was weaker at higher velocities for the exposure time of 1 s

significant variation in the exit position for the 10 µm sized beads. By increasing the shuffle flow volume and increasing the driving voltage from 8 V_{pp} to 10 V_{pp}, the deviation in exit positions was noticeably reduced. A larger

significant variation in the exit position for the 10 µm sized beads. By increasing the shuffle flow volume and increasing the driving voltage from 8 V_{pp} to 10 V_{pp}, the deviation in exit positions was noticeably reduced. A larger shuffle flow shifts the particles' entrance position relative the transducer in this case to a more favorable trajectory across the acoustic potential landscape over the transducer

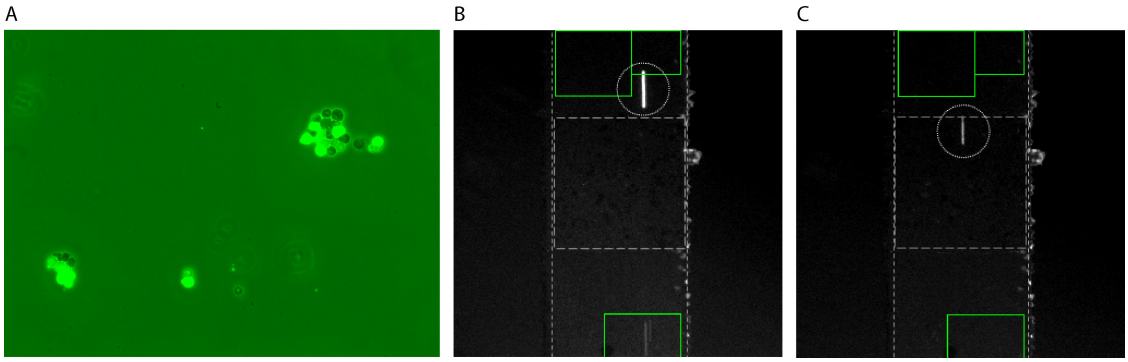

Figure 8. The µFACS-system was tested with E-GFP expressing β-cells. (A) About 50 % of the cells were expressing the fluorescence with slightly different intensities. (B) Images from the software program controlling the automated system showing a non-sorted β-cell and (C) a sorted β-cell.

Table 1. Evaluation of the automatic detection and sorting in terms of number of beads i) without transducer activation, ii) displacement of every bead, and iii) displacement of every second bead. The fluid flow is 3.4 mm s^{-1}.

Manually counted	Sorting algorithm	Detection zone A	Detection zone B	Detection zone C
100 (19.6 beads min^{-1})	no sorting	99	0	94
100 (28.0 beads min^{-1})	all sorted	99	100	7
100 (22.0 beads min^{-1})	every 2^{nd} sorted	98	50	49

surface (xy-direction). The potential landscape varies across the transducer surface and may yield differences in efficiency of the pre-alignment and the displacement. When increasing the driving voltage care must be taken to avoid acoustic trapping. By this fine-tuning of the parameters, the larger shuffle flow set-up resulted in improved pre-alignment (z-direction) and even at 25 mm s^{-1} flows, 10 µm particles were observed to have a joint exit position. For this higher driving voltage, the fluid displacement started already upstream the transducer. Compared to the measurements with smaller shuffle flow volume, the level of displacement was lower for flow velocities below 5 mm s^{-1}. Above 5 mm s^{-1}, the displacement was similar.

Few limitations exist regarding the type of cells that can be sorted. If the acoustic contrast factor is small, the pre-alignment (z-direction) effect is low and the flow speed needs to be reduced depending on the requirements of sorting yield. If on the other hand the acoustic contrast factor is large, the driving voltage may need to be lowered in order not to acoustically trap the cells above the transducer. An option is to include a 3D pre-focusing step prior to the acoustic zone, enabling the sorting of small particles, particles with low acoustic contrast factor and at high flow velocities. If increased sorting speed is of interest at the expense of a large displacement, a smaller channel width is expected to give a faster response.

Switch-time and automatic sorting evaluation

The automatic detection-and-switching step was evaluated in terms of switch-time at continuous operation and yield for the automatic sorting. The time required for fluid motion build-up to successfully shift a particle, i.e. the switch time, was found to be 0.36 s for the fluid flow of 3.4 mm s^{-1}, corresponding to approximately 3 particles s^{-1}.The fluid response time limits the speed in addition to the size of the transducer surface. This response time positions this device among the slower sorting methods mentioned in the introduction. In the automatic evaluation, a speed limitation of 0.3 s exists for the operation of the function generator. However, due to arrival statistics the sorting speed in practice is lower (0.5 particles s^{-1}). The detection yield was evaluated without acoustic switching for 100 manually counted particles, Table 1. The automatic sorting yield was evaluated by shifting every identified bead and every second identified bead. Compared to manual counting the statistical results in Table 1 show acceptable degrees of identification for the present optical set-up (>94

%). The number of identified particles in zone B plus zone C differed for a few events from the number of particles identified in zone A. The main reason is believed to be that two particles were too close to each other in the sample flow. This may result in two particles being registered as one in zone *A* which travel at different heights, i.e. with different speeds, may be registered as two in zone *C*. Alternatively they may be registered in zone B and C if the second particle is affected by the acoustic signal for only a part of the activation time and hence is displaced to a lower degree. The possibility of a second particle catching up with the first particle also exists.

Fluorescence activated cell sorting

E-GFP expressing β-cells were used as example cells for evaluating the system for its biological cell sorting capability. The MIN6 β-cells are 10-15 µm in size and ~ 50 % of the cells were expressing the GFP with a slight variation in intensity (Figure 8A). DPBS buffer was used both as cell suspension media and for the positioning fluids to attain a cell friendly environment. The single β-cells responded well to transducer activation (Figure 8B and 8C) with displacements similar to bead handling. Neither was acoustic trapping of the cells experienced at the used driving voltage (8 V_{pp}), nor were the β-cells non-specifically adsorbed to the channel walls to any noticeable extent. If a more biocompatible shuffle fluid is needed, a dextran solution of suitable concentration may be used.

The demonstrated ability to sort biological single-cells makes the presented µFACS-system suitable in applications for sorting or pre-concentration of cells in relatively small sample volumes. Examples are in the area of early cancer diagnostics, where cancer cells need to be sorted from healthy cells before culturing. A low-cost system would enable a larger number of patients to be screened at earlier stages. Cancer patients also need individual cytostatic immunity screening,[1, 39] where a miniaturized sorting system would be needed. Other examples include monoclonal antibody production where the µFACS-system could find a good application if hybridoma cells producing the sought after antibody could be identified by surface-bound antibodies or equally.[40] Stem cell-sorting, intracellular screening of blood cells for e.g. malaria parasites, or studies of cellular responses upon inserted mutations or various stimuli are other possible applications.[1] The gentleness of the acoustic switch makes it especially useful in applications for mammalian cells where viability in the following step is required, such as for transplantation. Also, beads can be functionalized to bind and extract smaller cells or analytes of interest from a larger mixture and the beads could be sorted from the solution for further analysis.

CONCLUSIONS

Successful cell and particle sorting by acoustic radiation forces at a fluid-fluid density interface is demonstrated. The acoustic wave originates from a miniaturized transducer that is fabricated into a printed circuit board, constituting the channel bottom, which makes the system simple to integrate with a wide selection of microfluidic channel designs. Large displacements were demonstrated and the system shows high flexibility regarding the kind of particles or cells to be sorted. The sorting mechanism also enables high flexibility regarding the cell medium. The described acoustic sorting method is expected to be gentle and thereby especially suitable for handling viable and sensitive cells when sorting speed is not the primary concern. At constant transducer activation and with 220 µm cell displacement, a sorting speed of 27 cells s^{-1} is obtained for a sample concentration with exactly one cell above the transducer at any time. Automated switching of the transducer, controlled by fluorescence signals from detected cells, showed that the system is useful not only for enrichment but also for high purity sorting. Based on maximum fluid displacement, the switch time is measured to 0.36 s corresponding to a sorting speed of approximately 3 particles s^{-1}.

ACKNOWLEDGEMENTS

We thank Anders Tengholm and co-workers at the Dep. of Medical Cell Biology, Uppsala University, for applying the MIN6 β-cells. Prof. Anders Larsson and Prof. Kjell-Olov Grönvik are acknowledged for valuable discussions.

REFERENCES

(1) Leary, J. F. *Cytometry Part A* **2005**, *67A*, 76-85.
(2) Fu, A. Y.; Chou, H. P.; Spence, C.; Arnold, F. H.; Quake, S. R. *Analytical Chemistry* **2002**, *74*, 2451-2457.
(3) Wolff, A.; Perch-Nielsen, I. R.; Larsen, U. D.; Friis, P.; Goranovic, G.; Poulsen, C. R.; Kutter, J. P.; Telleman, P. *Lab on a Chip* **2003**, *3*, 22-27.
(4) Wang, M. M.; Tu, E.; Raymond, D. E.; Yang, J. M.; Zhang, H. C.; Hagen, N.; Dees, B.; Mercer, E. M.; Forster, A. H.; Kariv, I.; Marchand, P. J.; Butler, W. F. *Nature Biotechnology* **2005**, *23*, 83-87.
(5) Sun, Y.; Lim, C. S.; Liu, A. Q.; Ayi, T. C.; Yap, P. H. *Sensors and Actuators a-Physical* **2007**, *133*, 340-348.
(6) Dittrich, P. S.; Schwille, P. *Analytical Chemistry* **2003**, *75*, 5767-5774.
(7) Johann, R.; Renaud, P. *Electrophoresis* **2004**, *25*, 3720-3729.

(8) Gomez, F. A. *Biological applications of microfluidics*, 1 ed.; John Wiley & Sons, Inc.: Hoboken, 2008.
(9) Yamada, M.; Nakashima, M.; Seki, M. *Analytical Chemistry* **2004**, *76*, 5465-5471.
(10) Huang, L. R.; Cox, E. C.; Austin, R. H.; Sturm, J. C. *Science* **2004**, *304*, 987-990.
(11) Lin, C. C.; Chen, A.; Lin, C. H. *Biomedical Microdevices* **2008**, *10*, 55-63.
(12) MacDonald, M. P.; Spalding, G. C.; Dholakia, K. *Nature* **2003**, *426*, 421-424.
(13) Lee, G. B.; Lin, C. H.; Chang, S. C. *Journal of Micromechanics and Microengineering* **2005**, *15*, 447-454.
(14) Petersson, F.; Aberg, L.; Sward-Nilsson, A. M.; Laurell, T. *Analytical Chemistry* **2007**, *79*, 5117-5123.
(15) Kang, J. H.; Park, J. *APBN* **2005**, *9*, 1135-1146.
(16) Neuman, K. C.; Chadd, E. H.; Liou, G. F.; Bergman, K.; Block, S. M. *Biophysical Journal* **1999**, *77*, 2856-2863.
(17) Dholakia, K.; Reece, P.; Gu, M. *Chemical Society Reviews* **2008**, *37*, 42-55.
(18) Jess, P. R. T.; Garces-Chavez, V.; Smith, D.; Mazilu, M.; Paterson, L.; Riches, A.; Herrington, C. S.; Sibbett, W.; Dholakia, K. *Optics Express* **2006**, *14*, 5779-5791.
(19) Fu, A. Y.; Spence, C.; Scherer, A.; Arnold, F. H.; Quake, S. R. *Nature Biotechnology* **1999**, *17*, 1109-1111.
(20) Chiou, P. Y.; Ohta, A. T.; Wu, M. C. 2005; pp.83-84.
(21) Petersson, F.; Nilsson, A.; Holm, C.; Jonsson, H.; Laurell, T. *Analyst* **2004**, *129*, 938-943.
(22) Nilsson, A.; Petersson, F.; Jonsson, H.; Laurell, T. *Lab on a Chip* **2004**, *4*, 131-135.
(23) Hawkes, J. J.; Barber, R. W.; Emerson, D. R.; Coakley, W. T. *Lab on a Chip* **2004**, *4*, 446-452.
(24) Hawkes, J. J.; Barrow, D.; Coakley, W. T. *Ultrasonics* **1998**, *36*, 925-931.
(25) Harris, N. R.; Hill, M.; Beeby, S.; Shen, Y.; White, N. M.; Hawkes, J. J.; Coakley, W. T. *Sensors and Actuators B-Chemical* **2003**, *95*, 425-434.
(26) Evander, M.; Horsman, K. M.; Easley, C. J.; Landers, J. P.; Nilsson, J.; Laurell, T. **2006**.
(27) Gaida, T.; DoblhoffDier, O.; Strutzenberger, K.; Katinger, H.; Burger, W.; Groschl, M.; Handl, B.; Benes, E. *Biotechnology Progress* **1996**, *12*, 73-76.
(28) Jagannathan, H.; Yaralioglu, G. G.; Ergun, A. S.; Khuri-Yakub, B. T. A.-K.-Y., B.T. 2003; 104-107.
(29) Hultstrom, J.; Manneberg, O.; Dopf, K.; Hertz, H. M.; Brismar, H.; Wiklund, M. *Ultrasound in Medicine and Biology* **2007**, *33*, 145-151.
(30) Bazou, D.; Foster, G. A.; Ralphs, J. R.; Coakley, W. T. *Molecular Membrane Biology* **2005**, *22*, 229-240.
(31) Evander, M.; Johansson, L.; Lilliehorn, T.; Piskur, J.; Lindvall, M.; Johansson, S.; Almqvist, M.; Laurell, T.; Nilsson, J. *Analytical Chemistry* **2007**, *79*, 2984-2991.
(32) Johansson, L.; Johansson, S.; Nikolajeff, F.; Thorslund, S. *Lab on a Chip* **2008**, DOI:10.1039/B815114H.
(33) Harris, N. R.; Hill, M.; Townsend, R.; White, N. M.; Beeby, S. P. *Sensors and Actuators B-Chemical* **2005**, *111*, 481-486.
(34) Wiklund, M.; Gunther, C.; Lemor, R.; Jager, M.; Fuhr, G.; Hertz, H. M. *Lab on a Chip* **2006**, *6*, 1537-1544.
(35) Meng, E.; Li, P. Y.; Tai, Y. C. In *Journal of Micromechanics and Microengineering*, 2008; Vol. 18, pp -.
(36) Johansson, L.; Johansson, S.; Nikolajeff, F.; Thorslund, S. *Lab on a Chip* **2009**, *9*, 297-304.
(37) Bruus, H. *Theoretical microfluidics*; Oxford University Press: Oxford, 2008.
(38) Wiklund, M.; Hertz, H. M. *Lab on a Chip* **2006**, *6*, 1279-1292.
(39) Ignatiadis, M.; Georgoulias, V.; Mavroudis, D. *European Journal of Cancer* **2008**, *44*, 2726-2736.
(40) Koster, S.; Angile, F. E.; Duan, H.; Agresti, J. J.; Wintner, A.; Schmitz, C.; Rowat, A. C.; Merten, C. A.; Pisignano, D.; Griffiths, A. D.; Weitz, D. A. *Lab on a Chip* **2008**, *8*, 1110-1115.